Joint Structures Determined by Clustering Microearthquakes Using Waveform Amplitude Ratios

Adam Roff , W. Scott Phillips and Donald W. Brown
Earth and Environmental Sciences Division
Los Alamos National Laboratory
Los Alamos, New Mexico 87545

International Journal of Rock Mechanics and Mining Sciences and Geomechanics Abstracts

Abstract

A new method of clustering seismic events has been developed to identify features within a large cloud of microearthquakes induced by the pressurization of a 3.5-km deep, jointed region of granitic rock. The relative amplitudes of shear- and compressional-waves were taken as an expression of the source mechanism for each microearthquake. Then, the events were clustered according to their similarity in S/P ratio and a second criterion, their spatial proximity to each other. Thus, each cluster contains events with closely spaced hypocenters and similar S/P ratios, and therefore a high probability of the same (or very similar) focal mechanism. This method was applied to a data set of 8,000 microearthquakes recorded during hydraulic stimulation of the Hot Dry Rock geothermal reservoir at Fenton Hill, New Mexico, located on the western flank of the Valles Caldera. Over 50 clusters of more than 10 events each were identified as planar features and over 20 such clusters were identified as linear features, together containing 15% of the usable events. Two predominant sets of planar features strike north to N45°W, roughly tangent to the ring fault system circling the caldera and dip 60° in either direction. These planes represent joints that may be associated with stress fields accompanying caldera formation. Most observed planes contain significant resolved shear within the current stress field. However, wide ranges of equally probable orientations are not observed, indicating a relatively unbiased sampling of the actual range of joint orientations. Most linear features are oriented parallel to one or both sets of planar features

and may be associated with joint intersections or terminations. These results support a reservoir flow model composed of water storage within aseismic joints oriented perpendicular to the minimum stress direction and of limited dimension, connected by high impedance paths along joints striking north to N45°W as defined by the cluster results.

Introduction

Microearthquakes recorded in seismically active regions can provide useful information about subsurface structures. However, it is often difficult to glean much structural detail from a plot of the hypocenters alone. Scatter in the hypocenter locations obscures features that are close together, and visualization of three-dimensional features in a two-dimensional scatter plot is often difficult. Even with perfect hypocenter locations, it would still be difficult to identify features in a cloud of many thousands of microearthquakes.

Within the last eight years, several techniques have been developed to discern structural details within such clouds of microseismic events. One recent method employs an iterative technique of moving event hypocenters around within their error ellipsoids in an attempt to concentrate, or focus, diffuse seismicity [1]. The 3-point method of Fehler [2] looks for planar features in an event cloud by taking all combinations of events three at a time to find all possible orientations of planes within the data set. A statistical analysis then identifies the most significant planar orientations given that some orientations will merely be artifacts of the overall shape of the seismic cloud. These methods [1,2] rely solely on the locations of the event hypocenters to define features in the event cloud. Modified versions of the 3-point method [3,4] use fault-plane solution data along with identified plane orientations of aftershocks to identify which of two nodal planes was the slip plane

of a main shock. This is a useful advance as both structure and mechanism can be inferred from the results.

An alternative approach to these methods is to first collect groups of events with similar focal mechanisms, and then look for patterns defined by their hypocenters. One method of identifying similar events is through waveform cross-correlation across all possible event pairs in the data set, so that events with high correlation can be grouped together. An advantage to this approach is that event timing and location can be improved in parallel. However, the cross-correlation and timing improvement process can be computationally intensive for large data sets [5].

The method we have developed uses the ratio of the first-arrival S- to P-wave amplitudes (S/P) at a given station as an expression of the earthquake focal mechanism. Using this less sophisticated measure of similarity between microearthquakes to selectively cluster events, we were able to identify numerous features within the microseismic cloud with much less coding and computational time than would have been required using waveform cross-correlation techniques.

In this paper we describe the application of this new method of analysis to a large data set of microearthquakes that were induced during the 1983 massive hydraulic fracturing (MHF) test performed at the Los Alamos National Laboratory's Fenton Hill Hot Dry Rock (HDR) test site in north-central New Mexico (Figure 1). In this

experiment, 21,600 m^3 of water was injected in 62 hours into a packer-isolated, 21-m section of openhole wellbore at a depth of 3460 m. The mean pumping conditions were a flow rate of 106 l/s at a wellhead pressure of 48 MPa.

We begin our discussion with the motivation for this new method of microseismic data analysis and then explain in detail how the method was applied to our particular data set. The results from this analysis consist of a large number of microearthquake clusters that are subsets of the total data set. Many of these clusters delineate planar and linear features that appear to be related to preexisting joints along which slip was induced. We anticipate that knowledge of the joint structure will help us to understand fluid flow through the reservoir.

Background

The amplitudes of P- and S-waves observed from an earthquake are affected by source parameters such as fault-plane orientation and slip vector, as well as take-off angle of the ray to the observer and the mechanical properties of the medium between the source and receiver. For events that are close together, the ratio of S- to P-wave amplitude remains a strong function of the source parameters, but is less affected by event size and raypath differences and can be used as a measure of a microearthquake's focal mechanism. Unfortunately, the relationship between S/P ratio and focal mechanism is not a unique one because different focal

mechanisms can lead to the same S/P ratio at a particular observation point. Furthermore the relationship is highly nonlinear, especially close to nodal regions in the P-wave radiation pattern. Nevertheless, closely spaced earthquakes with similar focal mechanisms should have similar S/P ratios at the same receiver.

Data

The microearthquake data set that we analyzed was recorded during and immediately following the December 1983 MHF test at the Fenton Hill HDR test site. Seismic events were recorded by four downhole geophones (Figure 2) for 85 hours beginning at the start of injection. Only a total of 844 events were digitized during the experiment. Locations were obtained using P- and S-wave arrival times at the four stations [6]. Data were later retrieved from analog tapes, resulting in over 11,000 locatable events. Of these, the highest quality locations are plotted in Figure 3. To calculate S/P amplitude ratios for the cluster analysis, we used only the vertical component of the triaxial geophone station located at a depth of 2865 m in borehole EE-1. Some 8,037 events yielded unsaturated seismograms at EE-1. For these 8,037 events, the RMS velocity amplitude was calculated in a 10-ms window (approximately 1.5 periods) starting at the arrival time for both P- and S-waves. S/P ratios for the entire data set ranged from 0.27 to 93.0 with a median value of 1.57.

To validate our use of S/P ratios to identify distinct features within the microseismic cloud, we examined the S/P ratios for two

separate clusters of events that had been previously identified by eye. Figure 3c shows the locations of these two clusters within the seismic cloud. Figure 4 shows three representative vertical component seismograms for each of the two groups as recorded at station EE-1.

The seismograms show distinct differences between the two clusters, while exhibiting strong similarity within each cluster. Note specifically the difference between relative amplitudes of P- and S-waves for the two clusters. Figure 5 shows the distribution of the S/P ratio for all events in clusters 1 and 2. Although each cluster has a spread of S/P ratios, their distributions have distinct peaks. Our new method of analysis exploits these differences to separate the entire data set into clusters.

Method

Microearthquakes are clustered according to both their S/P ratios and their spatial proximity, in an attempt to group events that share similar source orientations and locations. To separate events, a single-link cluster analysis was used [7]. The precise algorithm is an equivalence class routine [8] which has been used to identify clusters of similar earthquakes in the Anza seismic gap [5].

In single-link analysis, a true or false measure of equivalence between two events determines whether or not they are included in the same cluster. However, an event in a cluster need only be

equivalent to *one* other event in the same cluster. In this way, clusters of events with broad distributions in S/P ratio (such as clusters 1 and 2) should be allowed to form. This is one advantage of using a single-link cluster analysis instead of other grouping strategies.

Our method used a single parameter (S/P ratio) to characterize each earthquake's focal mechanism. However, it is possible that events from widely separated areas of the reservoir could appear to be identical if we used only this parameter as the measure of equivalence. Since we were interested in the detailed internal structure of the reservoir, it was necessary to impose a maximum separation distance of 100 m before two events were considered for comparison.

The two-criterion clustering method is illustrated in Figure 6. Events 1-5 are all within the allowable separation threshold of at least one other similar event, and thus are clustered together. Event 6 is within the separation threshold of three of the clustered events but fails the source mechanism equivalence test with all of them (the indicated fault plane solutions). Event 7 passes the equivalence criterion but exceeds the separation threshold with all the clustered events.

The measure of similarity used between two events was based on their proximity in the S/P ratio distribution. For example, a similarity criterion of one percentile means that two events are

considered similar if less than 80 (1% of 8037) other events lie between them in the ordered list of S/P ratios. The use of percentiles helps to overcome the non-linear nature of the relationship between S/P ratio and source parameters.

If the criteria of S/P ratio similarity and maximum spatial separation are not set strictly enough, every event in the data set passes the equivalence test with one or more other events. This results in the formation of one large cluster containing all the events. However, if the selection criteria are too strict, many events do not pass the equivalence test with any other events and thus do not cluster at all and are discarded from the analysis. To avoid these two extremes, we began with a set of criteria at which all events clustered together (1 percentile and 100 m) and then incrementally tightened the S/P ratio requirements for clustering. At each increment, the events were re-clustered and any planar or linear clusters were saved. This process was continued until all events were saved or were discarded in insignificantly small clusters (10 or fewer events). The decision to save a cluster was based on the visual examination of the cluster using map and orthogonal cross-section views oriented according to the largest cluster dimension (Figure 7). Cluster dimensions and orientations were calculated by eigenvector analysis of the spatial covariance matrix,

$$\begin{matrix} x_i x_i & x_i y_i & x_i z_i \\ y_i x_i & y_i y_i & y_i z_i \\ z_i x_i & z_i y_i & z_i z_i \end{matrix}$$

where x_i, y_i and z_i are the coordinates of event i and the Einstein summation convention is implied [9]. Measures of planarity and linearity were also calculated,

$$planarity = 1 - \lambda_2/\lambda_3;$$

$$linearity = 1 - \lambda_1/(\lambda_2+\lambda_3),$$

where the λ_i are the eigenvalues in descending order of magnitude. These measures were not used as selection criteria at this stage.

Results

The set of clusters obtained using the single-link technique with progressively tighter similarity requirements were grouped into planar and linear features by restricting planarity and linearity measures to be greater than 0.7. This resulted in 53 planar and 23 linear clusters (Tables 1 and 2). Taking account of events in clusters common to both groups, the number of events in these clusters total about 1200, or 15% of the events available for analysis.

To view the spatial distribution of the planar clusters, the best fit plane through each cluster was bounded by the smallest in-plane rectangle with horizontal top and bottom edges that contained the projected hypocenter locations. A representative solid rectangle was formed by adding the same width to all rectangles (Figure 7). Figure 8 shows the same view looking west as in Figure 3c, but with the

representative solid rectangles replacing the hypocenter locations. The planes we identified appear in spatially distinct groups throughout the reservoir volume. This grouping of seismicity is also visible in the event hypocenter plot (Figure 3c).

Although the overall Fenton Hill seismicity forms a flattened, ellipsoidal volume striking approximately north (Figure 3), the majority of the planes located during the MHF test strike between north and N45°W and dip 60° or more, both to the east and west as indicated by the lower hemisphere projection of poles to planes (Figure 9a). Eastward dipping planes are twice as plentiful as westward dipping planes. Orientations of linear features are shown in Figure 9b. Most linear features trend roughly parallel to strikes of the predominant populations of planar features. Plunges are distributed in all directions with near horizontal being most common.

Discussion

The linear and planar features we identified are composed of about 1200 microearthquakes, so there still remain some 6800 other events that were discarded from the analysis. One reason for this is that high thresholds of similarity were needed to adequately split the data set into clusters. This results in narrow distributions of S/P ratio in the clusters produced (compare Figure 5 distributions with that in Figure 7). Tighter spatial constraints and looser S/P differences might have yielded larger numbers of events in clusters, but this was not investigated. Another reason is that routinely

determined locations were relied on and clusters may have been ignored because of lack of structure. Therefore, the 15% clustering obtained with the S/P ratio technique underestimates the degree of clustering in the data set. The use of waveform cross-correlation as the clustering parameter may also help to increase the degree of clustering. Waveforms carry more information than S/P ratios and thus the microearthquakes would be potentially more distinct from each other, yielding more clusters at low similarity thresholds. In addition, improvement in relative arrival times of clustered events would lead to lower relative location error and easy identification of structures. This technique should decrease the number of events that need to be discarded from the analysis. Although the computational burden will increase, the use of cross-correlation techniques have the potential to further our understanding of the detailed structure of the reservoir.

The Fenton Hill site sits on the western flank of the Valles Caldera at a point where the ring fault system strikes roughly N20°W (Figure 1), parallel to the mean strike of the two main families of planar features found by the cluster analysis. The planar features represent joints that may be associated with stresses that accompanied caldera emplacement or collapse. Furthermore, the most populous of the two observed planar families dips to the east, similar to the normal faults of the ring fault system closest to Fenton Hill.

The poles to the planes identified by application of the 3-point

method to an 844-event subset of the data from the same hydraulic stimulation experiment [2] show general agreement with those found by our analysis (Figure 10). The 3-point results indicate statistical trends of gross features in the data set, whereas clustering resolves the reservoir structure on a finer scale, both methods giving similar orientations.

A number of wellbore/plane intersections are apparent in Figure 8. The locations of two of these intersections correlate with independent information regarding the flow paths of high pressure water through the rock mass. The intersection of an inferred plane with the EE-2 wellbore at a depth of 3250 m coincides with a wellbore casing failure caused by a high pressure flow connection intersecting the wellbore at this point. The intersection of an inferred plane with the EE-3A wellbore around 3450 m is located in the openhole region through which high pressure water was being pumped when fluid connections to wellbore EE-2 were first achieved in the spring of 1986. The water flowing from EE-3A to EE-2 during this flow test would most likely have occurred along flow paths represented by interconnecting, previously opened joints. These coincident phenomena indicate that high pressure water is present along at least some if not all the identified joint planes.

Previous work on hydraulic fracturing at Fenton Hill indicates that shear-slip along preexisting joints in the rock mass is the major cause of seismicity [10]. The large S/P amplitude ratios and P-wave polarity changes we observe from the events support the concept of

a shear mechanism. To further understand the dynamics of our reservoir, it is important to compare observed planar orientations with the stress field. Stress measurements at Fenton Hill have been summarized as σ_1 vertical, σ_3 horizontal, N104°E, $\sigma_1/\sigma_2=2$, $\sigma_2/\sigma_3=1.5$, determined from pressurization and wellbore breakout data [11]. These directions match orientations expected for the Rio Grande Rift, although this area has been classified as a transition stress region with a range of measured principal stress orientations [12]. This stress field is also consistent with the overall orientation of Fenton Hill reservoir seismicity which fills a flattened, ellipsoidal volume (Figure 3), oriented roughly perpendicular to the minimum principal stress. As in [11] the ratio of resolved shear and normal stresses on a planar surface is plotted along with the observed planar orientations in Figure 10. The two predominant populations of planar features are oriented near the peak expected shear. However, the observations do not follow the maximum shear pattern perfectly and a significant number of observations fall well away from the peaks. Because wide ranges of equally probable orientations are not observed, we have confidence that the range of observations is a relatively unbiased estimate of the range of actual joint orientations. Exceptions to this would be joints oriented perpendicular to any of the principal stress axes.

Another reservoir stress model is tightly constrained by focal mechanisms of nearly 200 large events recorded during injection by a network of seismometers on the earth's surface, giving σ_1 horizontal, N155°E, σ_3 near vertical, $(\sigma_1-\sigma_2)/(\sigma_1-\sigma_3)=0.5$ [13]. This is

quite different from the model discussed above. Differences between focal mechanisms and pre-injection stresses were observed at Le Mayet de Montagne, France and were attributed to local perturbations in the stress field resulting from relaxation along a fault during fluid injection [14]. Qualitatively, we can not resolve the difference between the two stress fields because it is difficult to significantly reduce the vertical stress relative to the horizontal stresses using pressurization and shear relaxation ideas along joints striking north to N45°W. The similarity between the σ_1 direction from focal mechanisms and the strikes of the observed planar features may be a clue to the mechanism at work.

Linear features are also prevalent in the set of clusters found in the hydraulic stimulation data set. Linear clusters are identified as those with a long axis that is much larger than the other two. However, a cluster can be both linear and planar if the ratio of major and intermediate and the ratio of intermediate and minor axes are both large. Just under half of the linear features can be placed in both categories (see Tables 1 and 2). All linear clusters are oriented parallel to one or both sets of the observed planar features. We believe these features are expressions of joint intersections or terminations. A test was performed to compare the orientations of linear features with the distribution of planar intersections, taking all possible pairs of the observed planar orientations. The density of planar intersection orientations (per unit solid angle, radians) is normalized by the number of unique planar pairs and contoured in Figure 11. The observed orientations match the distribution of

planar intersections well, especially the near-horizontal features. A more detailed interpretation of the distribution of planar intersections must rely on the spatial uniformity of the joint distribution which may not be completely valid. The linear features that trend north or south are also consistent with intersections between cluster planes and any north-striking vertical joints oriented perpendicular to the minimum stress that may exist.

The earliest concept of the Hot Dry Rock reservoir at Fenton Hill consisted of fluid flow through a few large vertical fractures striking north, aligned perpendicular to the minimum principal stress. Initial analysis of seismic data resulted in the idea of multiple, diffuse fluid paths [6]. Later, results of the 3-point method [2] indicated the presence of large planar features in the reservoir. These planes were oriented for shear and were not oriented perpendicular to the minimum stress direction [11]. The many planar features identified by our method and their small size relative to the reservoir volume (Figure 8) imply that the reservoir consists of a jointed volume of rock, with no single fracture traversing the entire seismically active zone. This brings us to a model of the reservoir in which water is stored in aseismic joints striking north and dipping near vertical, perpendicular to the minimum principal stress (σ_3 horizontal, N104°E). The existence of such joints is supported by the gradual recovery of wellhead pressure to a level consistent with the magnitude of the minimum stress (10 MPa above hydrostatic) following reservoir venting [15], as well as by the growth of overall reservoir seismicity roughly perpendicular to the minimum stress

direction (Figure 3). These easily opened joints would be low impedance components of fluid flow paths and would be less likely to be observed seismically because there is little resolved shear. However, these joints do not extend uninterrupted for significant distances, otherwise flow communication between the initial pair of wellbores (EE-2 and EE-3) would have been easily established early in the project at low injection pressures of 10 to 15 MPa. It therefore appears that these storage joints are truncated by the joint sets inferred from microearthquake clusters that strike between north and N45°W and dip 60° in both directions. We envision a "rooftop" model of joints striking oblique to the water storage joints, providing tortuous, high impedance flow paths that connect storage joints and enable fluid to move large distances through the rock mass. The high impedance flow paths are consistent with the high pressures (about 27 MPa) required to pump a significant amount of water into the reservoir [15].

Conclusions

We have identified a large number of features in a cloud of microearthquakes generated by the pressure stimulation of a 3.5-km deep, jointed, Precambrian granitic rock mass. The locations and orientations of these features are defined by hypocenters of microearthquake clusters. Similarity in the S- to P-wave amplitude ratios of all microearthquakes in a given cluster implies a common slip mechanism. The co-planarity of the hypocenters in many of these clusters suggests planes along which pressure dilation and slip

is occurring. Most of these planes strike parallel to normal faults of the nearby ring fault system of the Valles Caldera. Of two sets of observed planes, the most populous dips to the east, similar to the caldera ring faults. Planes are smaller and more numerous, yet are similarly oriented to features found by applying a 3-point, statistical method to the microearthquake hypocenters [2]. Given estimates of the stress field from pressurization and wellbore breakouts, the observed planes are oriented well for shear. However, many high shear orientations are not observed, indicating that the range of observed orientations is a reasonably unbiased estimate of the range of actual joint orientations in the subsurface. Another estimate of stress is very well constrained by focal mechanisms of the largest microearthquakes, giving the maximum principal stress parallel to strikes of the observed planar features, but differences between the two stress estimates are difficult to resolve using pressure dilation and shear relaxation ideas. Linear features are also common in our set of microearthquake clusters and are related to joint intersections. The orientations of linear features are consistent with the distribution of intersections of all possible pairs of the observed planar features. From these results we envision a “rooftop” model of the reservoir with water storage in joints of limited dimension oriented perpendicular to the minimum stress. These joints are connected by high impedance flow paths through joints represented by the observed planar orientations, striking between north and N45°W and dipping 60° in both directions.

Acknowledgments

We would like to thank Leigh House, Mike Fehler, Norma McFarland and Rod Flores for their roles in providing the data used in our analysis and Ruth Bigio and Florence Fujita for their help with the figures. The paper has benefited greatly from reviews by Mike Fehler and two anonymous referees. Thanks also to Fred Moreno for discussions about caldera structure and to Jim Albright for describing early work on microearthquake waveform clustering. This work was supported by the U. S. Department of Energy, Office of Basic Energy Sciences, Division of Geosciences and Engineering under contract W-7405-ENG-36 and the Geothermal Technology Division through its Hot Dry Rock geothermal energy development program.

References

1. Jones R.H. and Stewart R.C. The structure of the active ring fault at Rabaul Caldera determined from an analysis of earthquake location errors. *EOS Trans. Am. Geoph. Un.* **74**, 402 (1993).

2. Fehler M., House L.S. and Kaieda H. Determining planes along which earthquakes occur : Method and application to earthquakes accompanying hydraulic fracturing. *J. Geophys. Res.* **92**, 9407-9414 (1987).

3. Fehler M.C. and Johnson P.A. Determination of fault planes at Coalinga, California, by analysis of patterns in aftershock locations. *J. Geophys. Res.* **94,** 7496-7506 (1989).

4. Fehler M. Identifying the plane of slip for a fault plane solution from clustering of locations of nearby earthquakes. *Geophys. Res. Lett.* **17,** 969-972 (1990).

5. Aster R. and Scott J. Comprehensive characterization of waveform similarity in microearthquake data sets. *Bull. Seism. Soc. Am.* **83**,1307-1314 (1993).

6. House L.H. Locating microearthquakes induced by hydraulic fracturing in crystalline rock. *Geophys. Res. Lett.* **14**, 919-921 (1987).

7. Davis, J.C. *Statistics and data analysis in Geology*, 2nd Edition, John Wiley & Sons, New York (1986).

8. Press W., Flannery B., Teukolsky S. and Vetterling J. *Numerical Recipes*, Cambridge University Press, Cambridge, U.K. (1986).

9. Flinn E.A. Signal analysis using rectilinearity and direction of particle motion. *Proc. IEEE* **53**, 1725-1743 (1965).

10. Pearson C. The relationship between microseismicity and high pore pressure during hydraulic stimulation experiments in low permeability granitic rocks. *J. Geophys. Res.* **86**, 7855-7864 (1981).

11. Fehler, M.C. Stress control of seismicity patterns observed during hydraulic fracturing experiments at the Fenton Hill Hot Dry Rock geothermal energy site, New Mexico. *Int. J. Rock Mech. Min. Sci. & Geomech. Abstr.* **26**, 211-219 (1989).

12. Aldrich, M.J., Chapin, C.E. and Laughlin, A.W. Stress history and tectonic development of the Rio Grande Rift, New Mexico. *J. Geophys. Res.* **91**, 6199-6211 (1986).

13. House, L.S. Personal communication (1995).

14. Scotti, O. and Cornet F.H. In Situ evidence for fluid-induced aseismic slip events along fault zones. *Int. J. Rock Mech. Min.*

Sci. & Geomech. Abstr. **31**, 347-358, (1994).

15. Brown, D.W. The potential for large errors in the inferred minimum earth stress when using incomplete hydraulic fracturing results. *Int. J. Rock Mech. Min. Sci. & Geomech. Abstr.* **26**, 573-577 (1989).

Figure Captions

Figure 1. Map showing the Valles Caldera area and the location of the Fenton Hill HDR geothermal site.

Figure 2. Locations of borehole geophone tools (filled circles) deployed during the MHF experiment. EE-1 and EE-3 are three-component tools while PC-1 and GT-1 are single-component vertical tools.

Figure 3. Three orthogonal views of MHF seismicity: a) map view, b) cross-section looking north, and c) cross-section looking west, with circles designating clusters 1 and 2 discussed in the text. Wellbores are indicated where they are not obscured by the seismicity. Wellheads are represented by filled circles.

Figure 4. Vertical component seismograms for three events each from clusters 1 (top three) and 2 (bottom three) versus time in seconds relative to the P-wave first arrival.

Figure 5. Distributions of the S/P ratio for example clusters 1 (triangles) and 2 (squares), normalized so that peak values are unity.

Figure 6. Illustration of the two-criteria clustering method.

Figure 7. One of the planar clusters identified by the S/P ratio

analysis. Counter-clockwise from bottom right : view along strike, rotated map view, view across strike, S/P ratio distribution for this cluster and temporal distribution of events in this cluster. Hypocenter plots also contain an outline of the solid rectangle used to view the spatial distribution of planar clusters.

Figure 8. Cross-section view looking west (as in Figure 3c) of the solid rectangles representing planar clusters. Note locations of plane-wellbore intersections and the wellbore failure.

Figure 9. Lower hemisphere, equal area projections of (a) poles to planar clusters and (b) axes of linear clusters identified by the S/P ratio method.

Figure 10. Lower hemisphere, equal area projection of poles to planar clusters (dots), poles to planar features identified by the 3-point method (triangles) and contours of the ratio of shear to normal stress acting on a plane as in [11]. Intermediate and minimum principal stress directions are noted, maximum principal stress is vertical.

Figure 11. Lower hemisphere, equal area projection of axes of linear features (dots) and contours representing the distribution of planar intersections as described in the text.

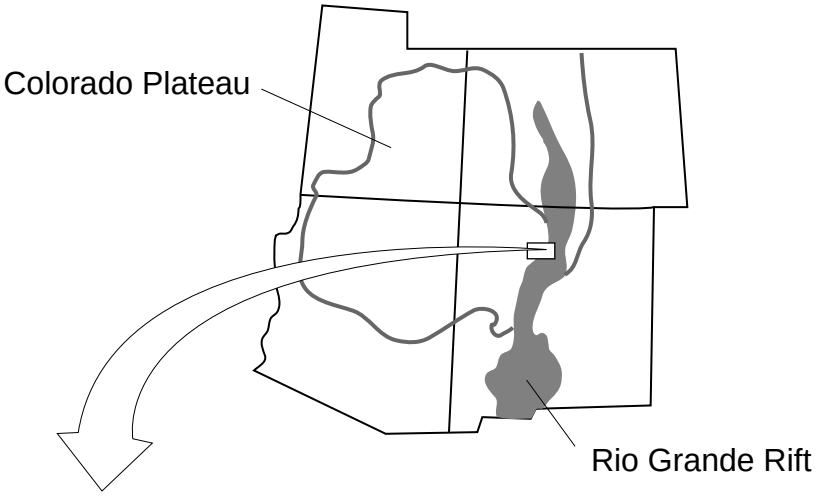
Colorado Plateau
Rio Grande Rift

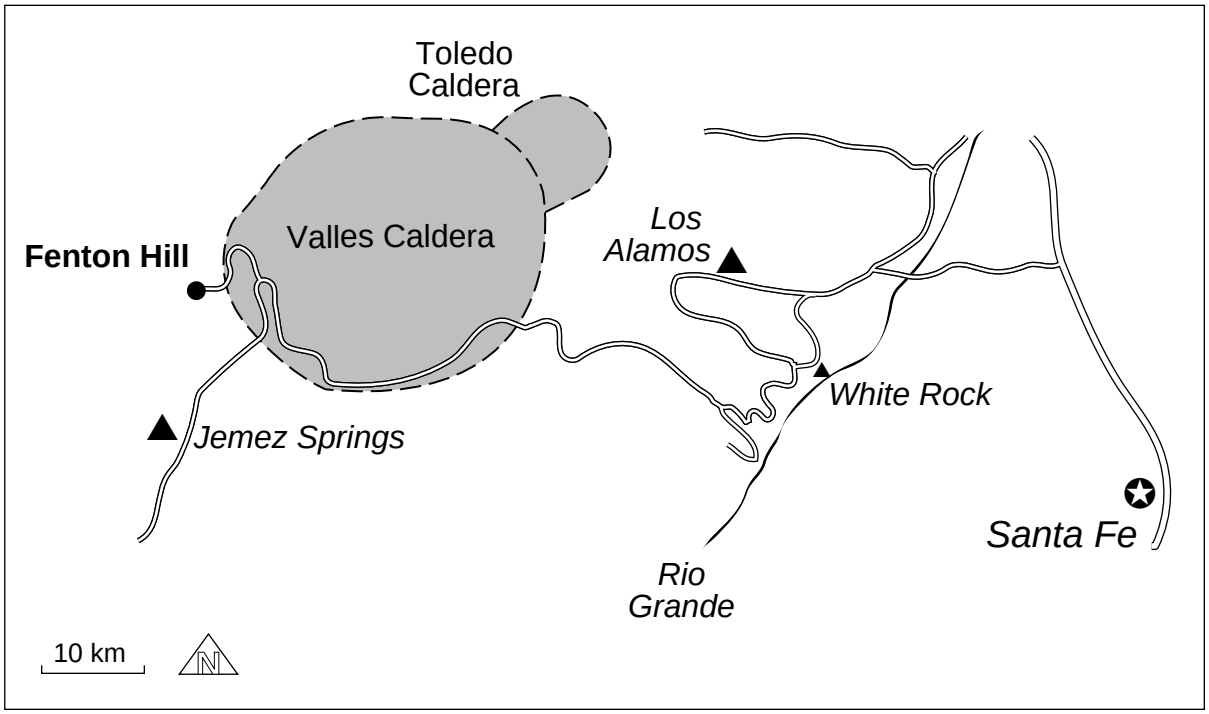
Toledo
Caldera
Valles Caldera
Fenton Hill
Los
Alamos
White Rock
Jemez Springs
Santa Fe
Rio
Grande
10 km
N

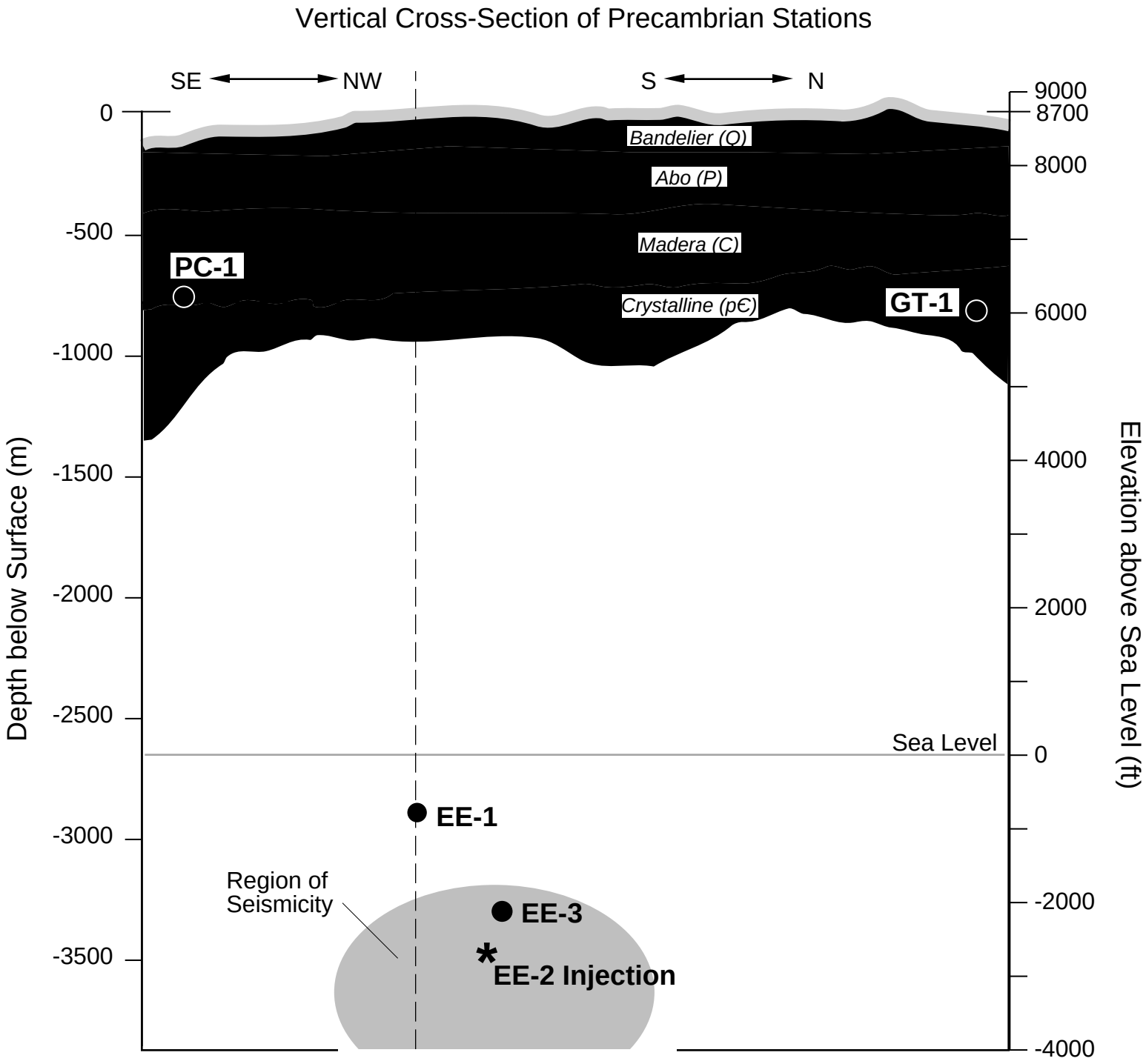
Vertical Cross-Section of Precambrian Stations
SE
NW
S
N
0
-500
-1000
-1500
-2000
-2500
-3000
-3500
9000
8700
8000
6000
4000
2000
0
-2000
-4000
Depth below Surface (m)
Elevation above Sea Level (ft)
Bandelier (Q)
Abo (P)
Madera (C)
Crystalline (pЄ)
PC-1
GT-1
Sea Level
EE-1
Region of
Seismicity
EE-3
EE-2 Injection

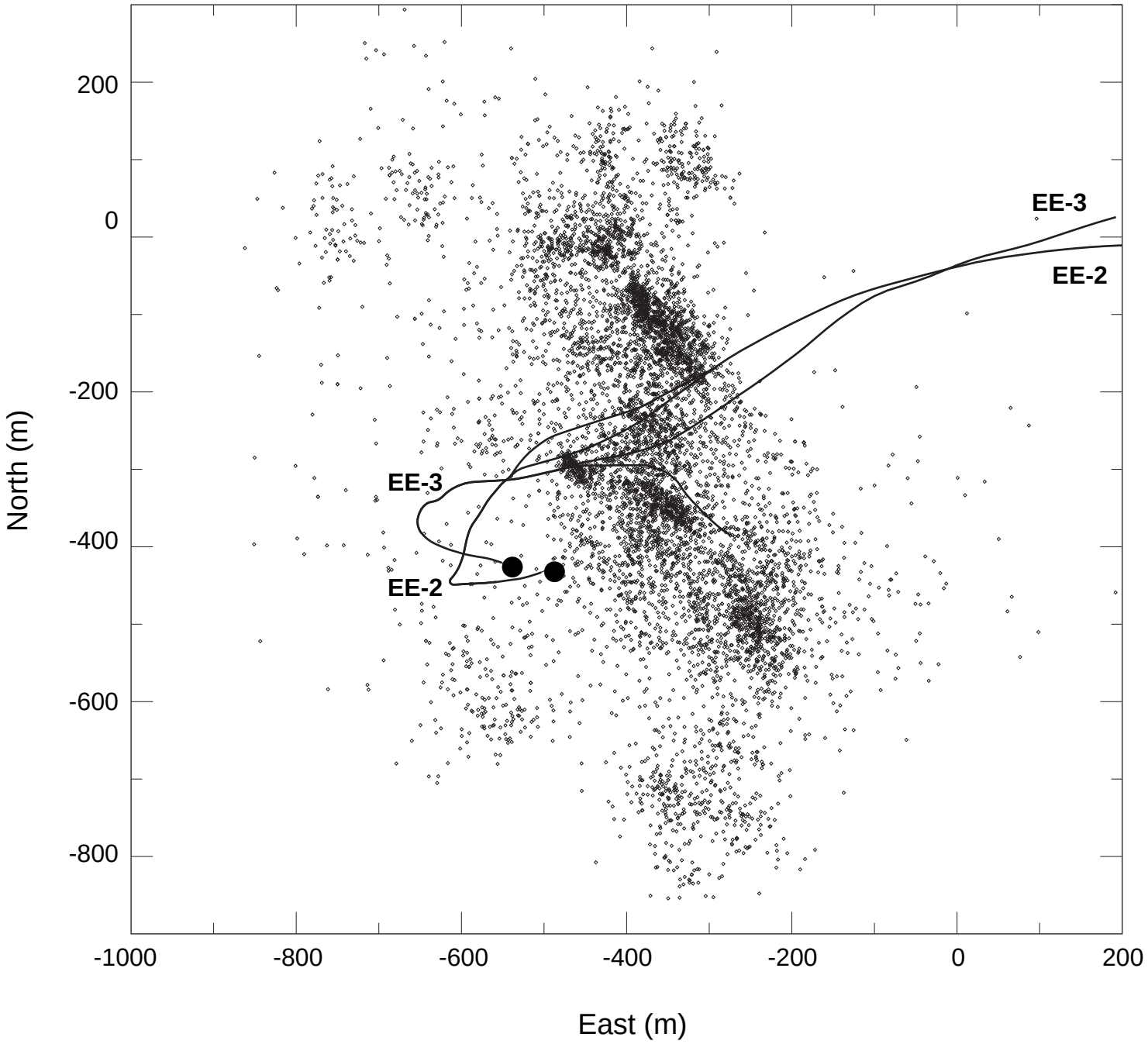
200
0
-200
-400
-600
-800
North (m)
-1000
-800
-600
-400
-200
0
200
East (m)
EE-3
EE-2
EE-3
EE-2

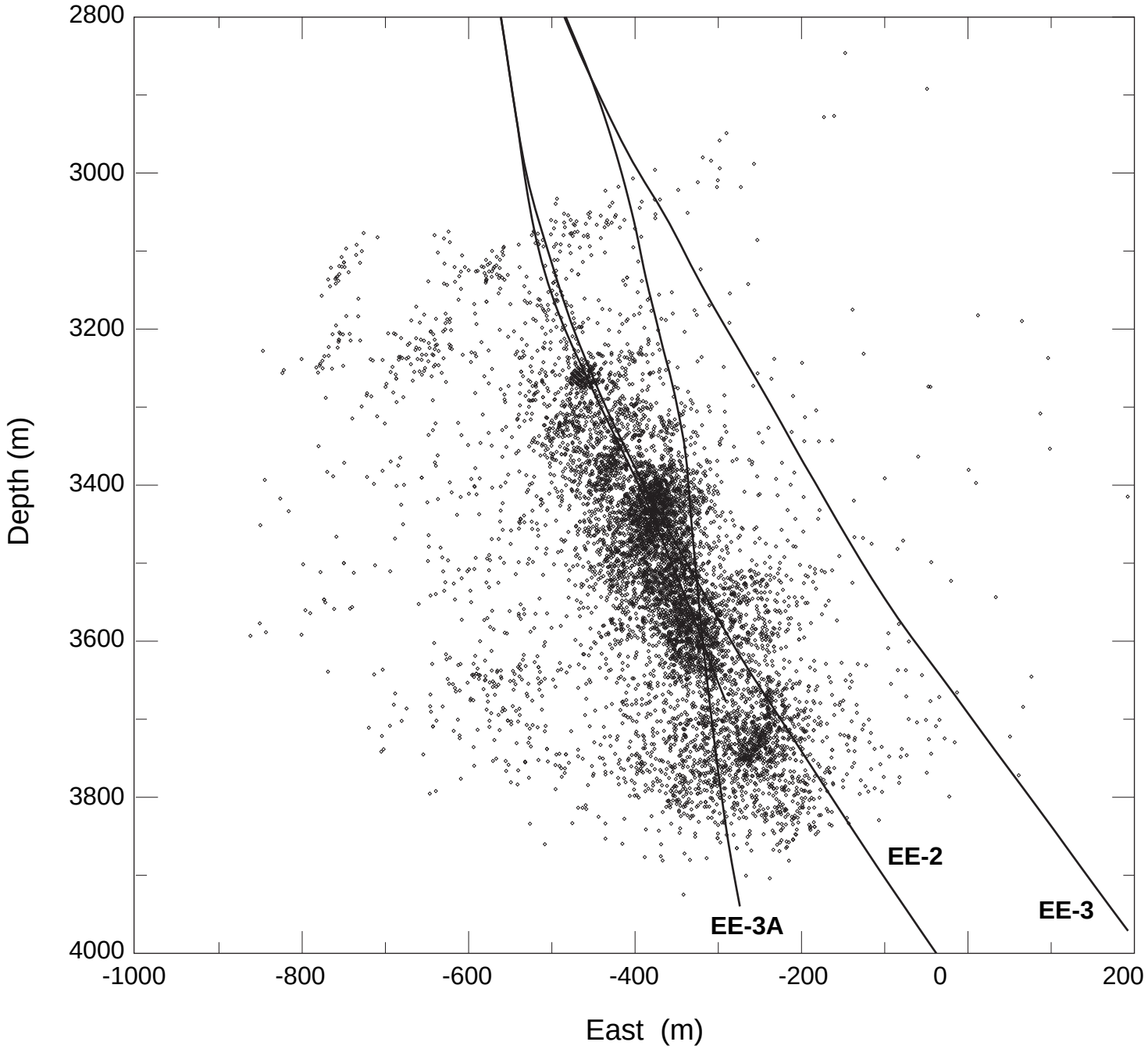
2800
3000
3200
3400
3600
3800
4000
Depth (m)
-1000
-800
-600
-400
-200
0
200
East (m)
EE-2
EE-3
EE-3A

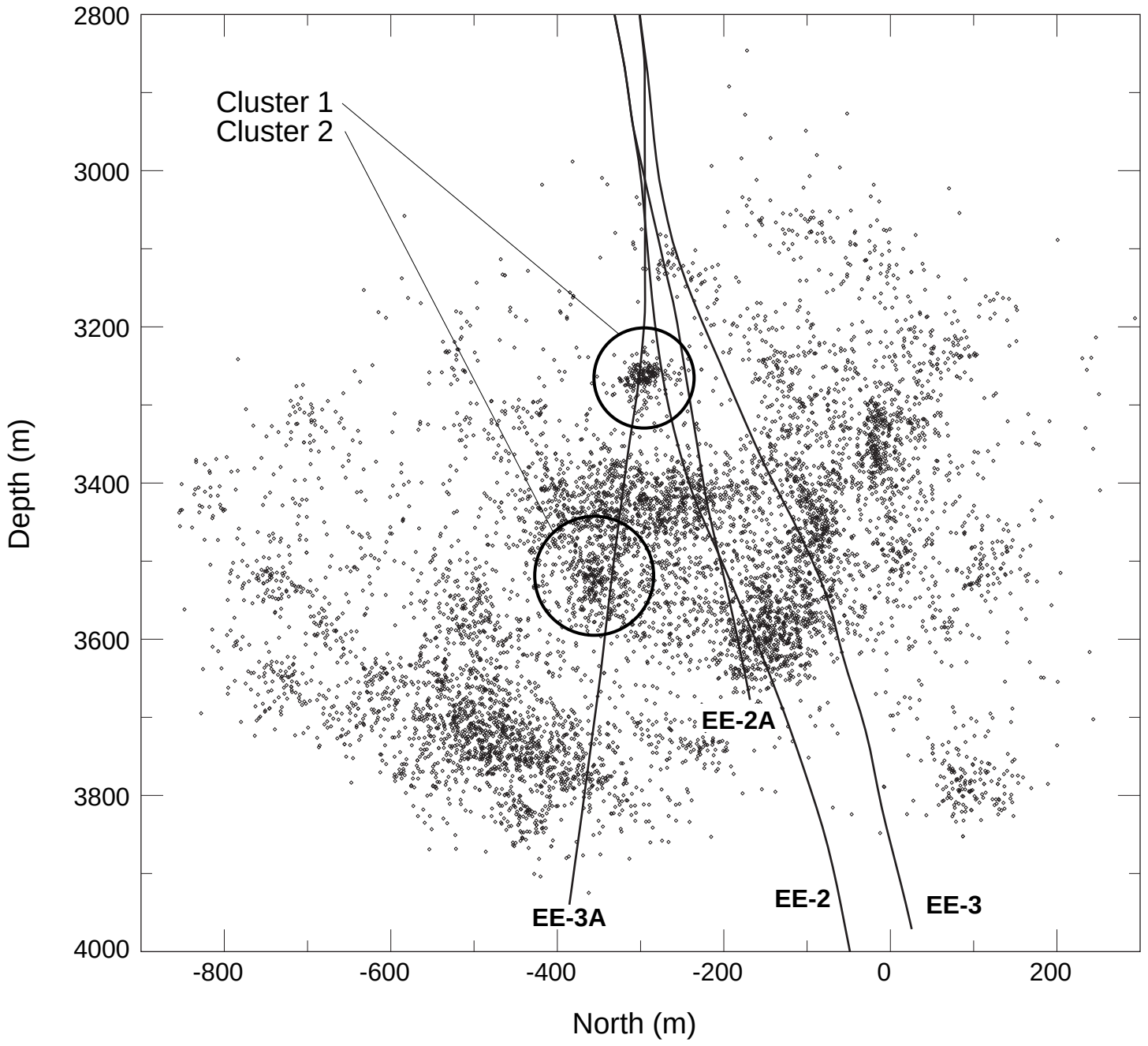
Cluster 1
Cluster 2
EE-2A
EE-3A
EE-2
EE-3
Depth (m)
North (m)
2800
3000
3200
3400
3600
3800
4000
-800
-600
-400
-200
0
200

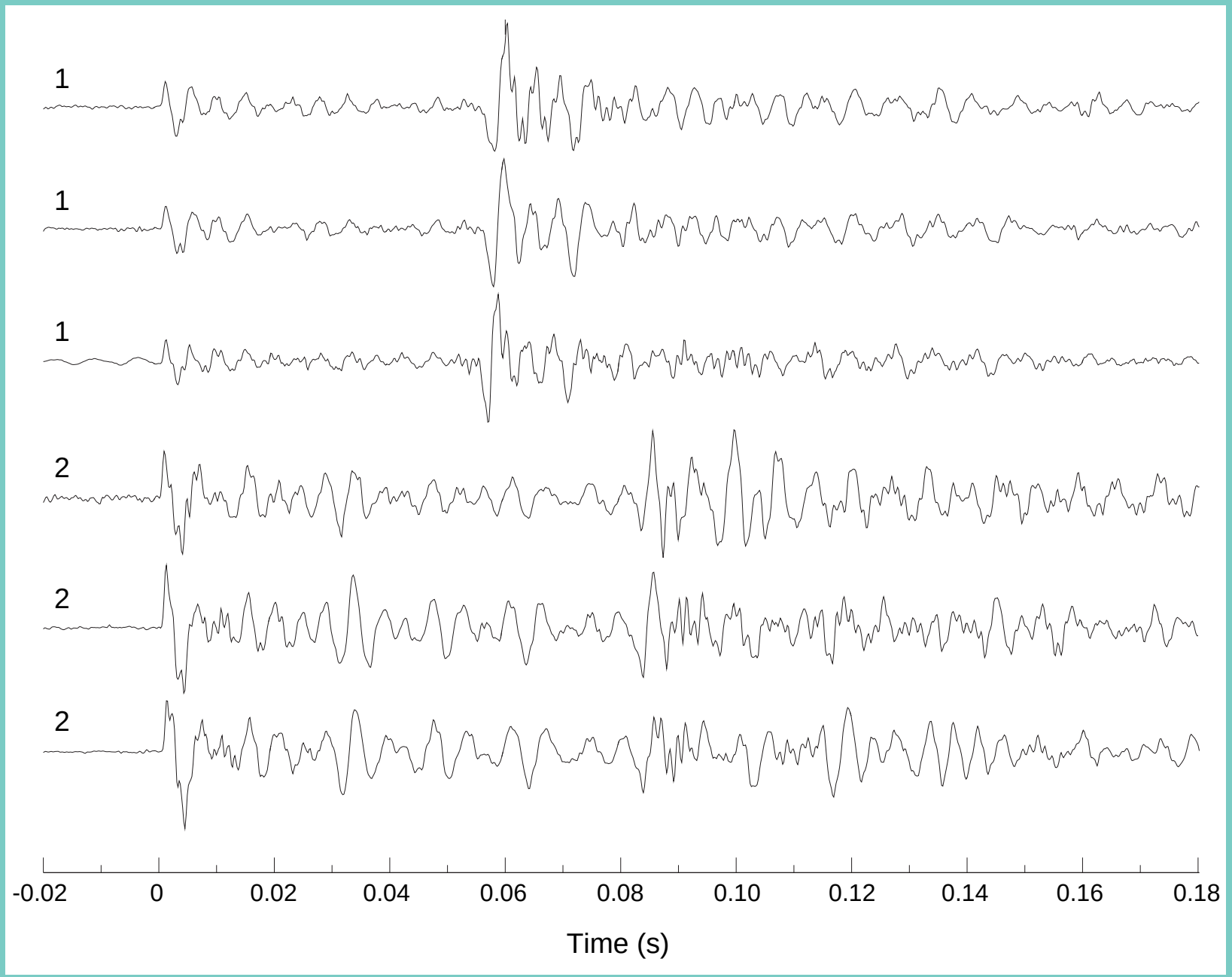
1
1
1
2
2
2
-0.02
0
0.02
0.04
0.06
0.08
0.10
0.12
0.14
0.16
0.18
Time (s)

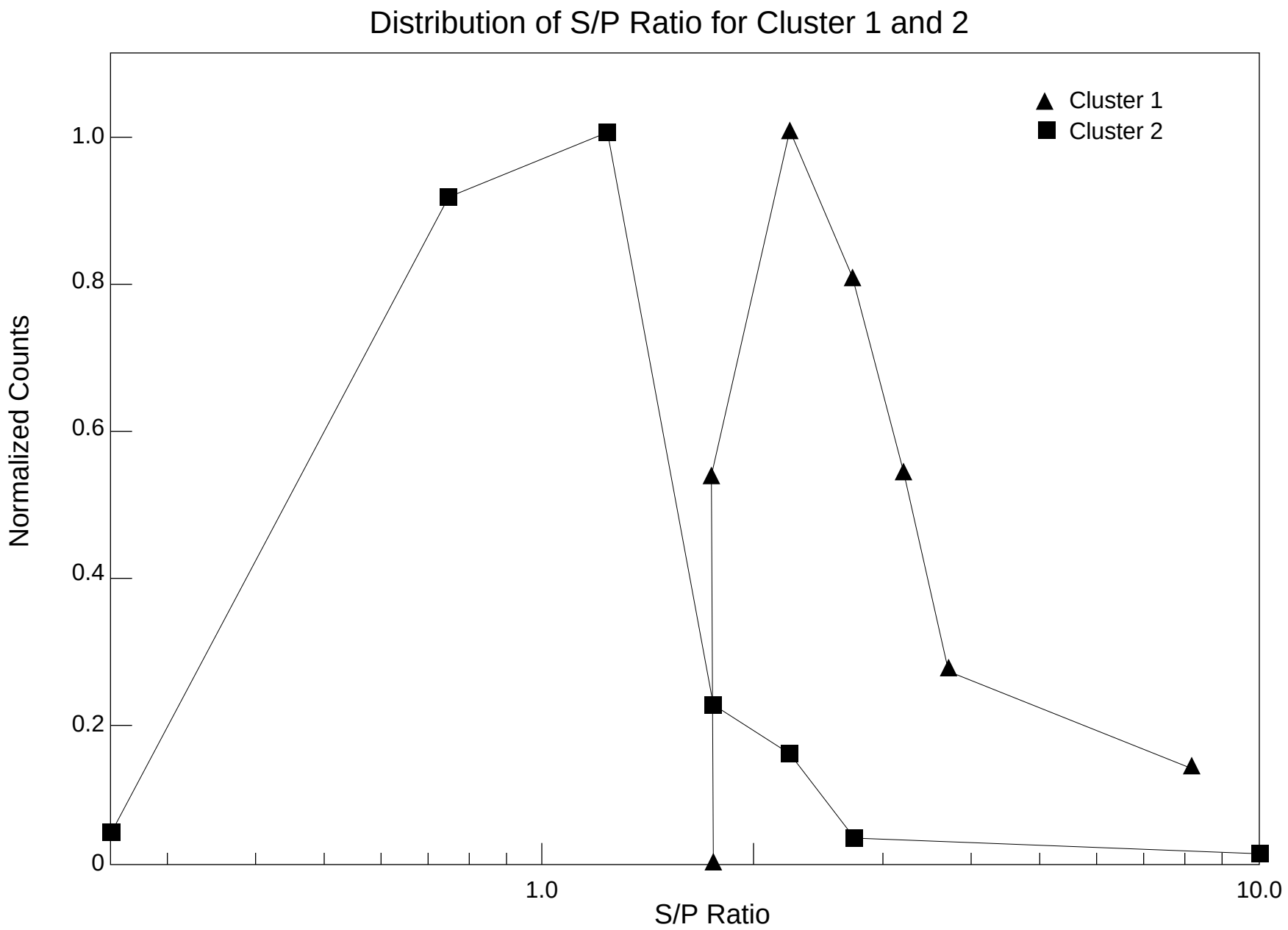
Distribution of S/P Ratio for Cluster 1 and 2
Cluster 1
Cluster 2
Normalized Counts
1.0
0.8
0.6
0.4
0.2
0
1.0
10.0
S/P Ratio

Clustering Example

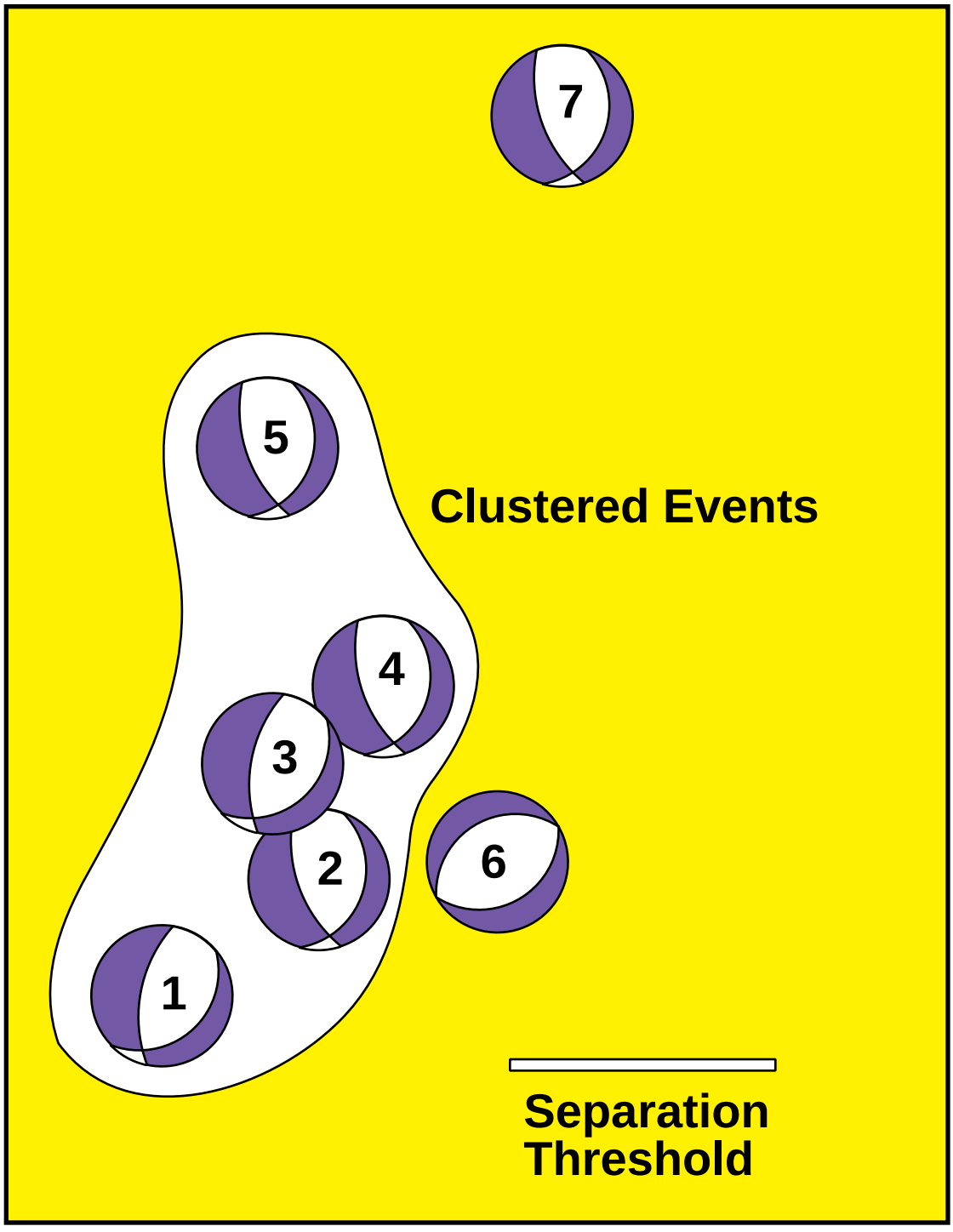

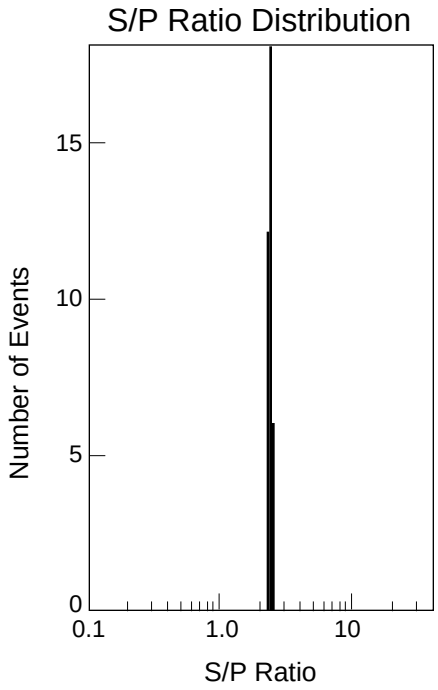
S/P Ratio Distribution
Number of Events
0
5
10
15
0.1
1.0
10
S/P Ratio

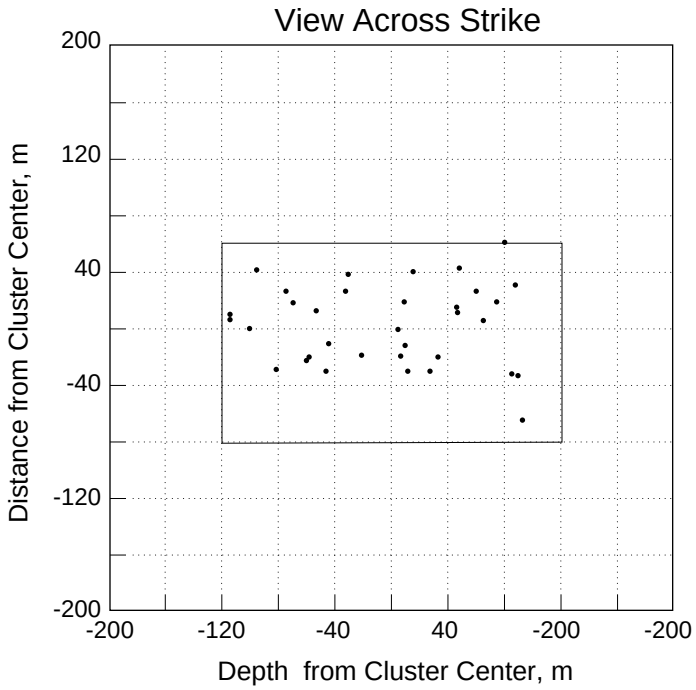
View Across Strike
Distance from Cluster Center, m
200
120
40
-40
-120
-200
-200
-120
-40
40
-200
-200
Depth from Cluster Center, m

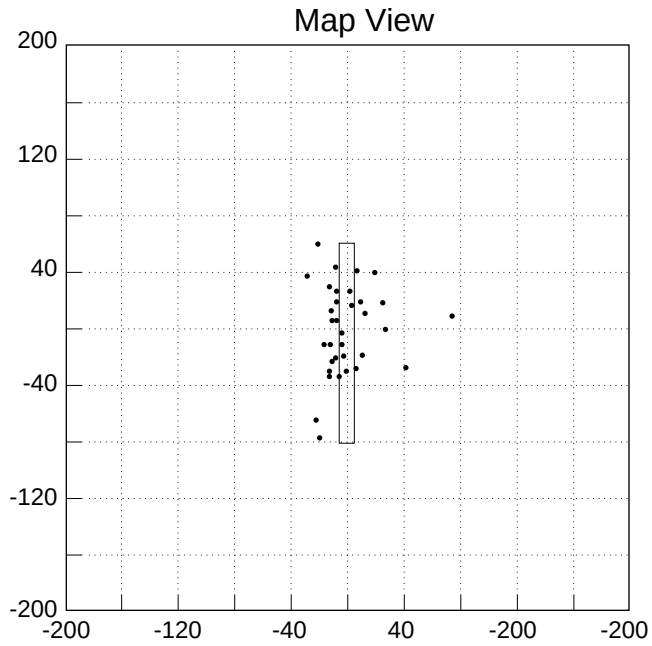
Map View
200
120
40
-40
-120
-200
-200
-120
-40
40
-200
-200


Number of Events/Hour Through Experiment
Number of Events
0
5
10
15
20
0
10
20
30
40
50
60
70
80
Hours from Start of Experiment

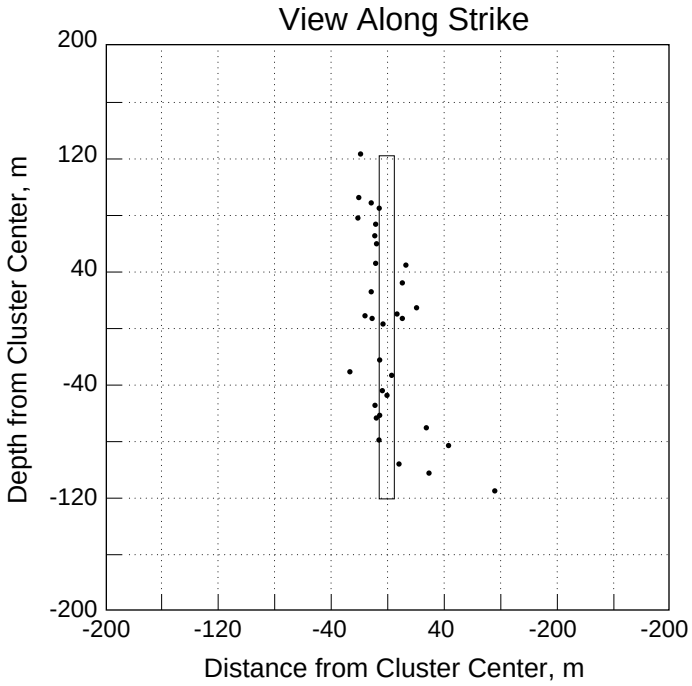
View Along Strike
Depth from Cluster Center, m
200
120
40
-40
-120
-200
-200
-120
-40
40
-200
-200
Distance from Cluster Center, m

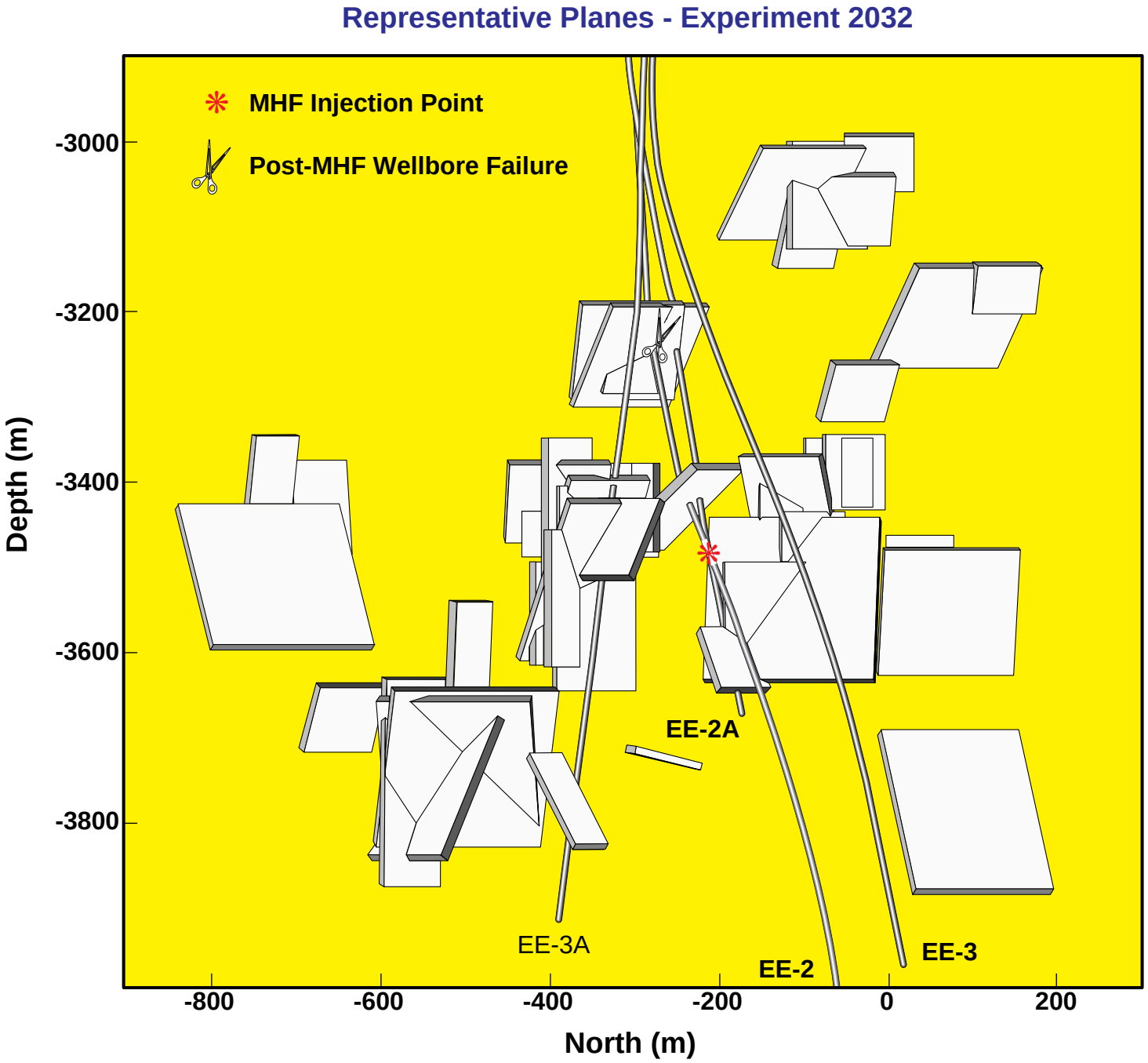
Representative Planes - Experiment 2032
MHF Injection Point
Post-MHF Wellbore Failure
Depth (m)
-3000
-3200
-3400
-3600
-3800
-800
-600
-400
-200
0
200
North (m)
EE-2A
EE-3A
EE-2
EE-3

a) Planar Features

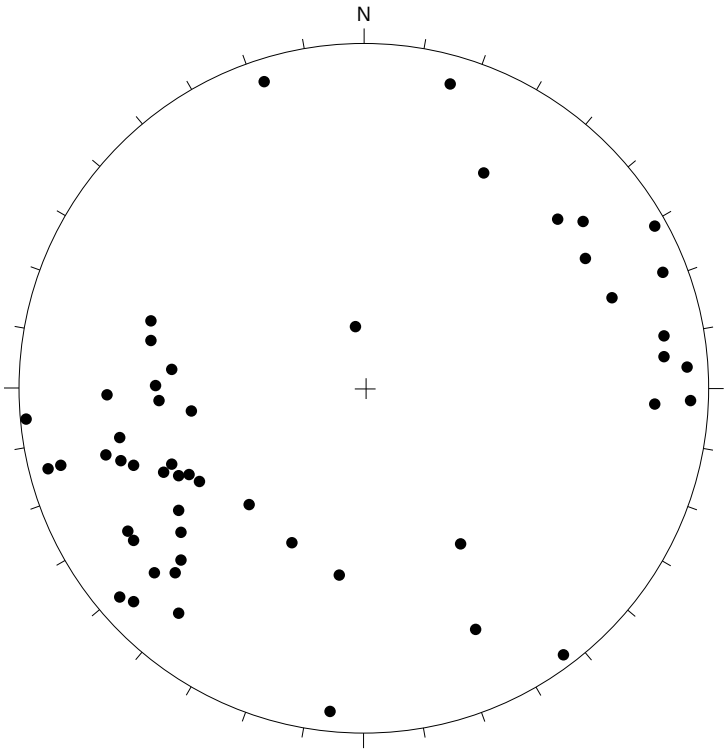

b) Linear Features

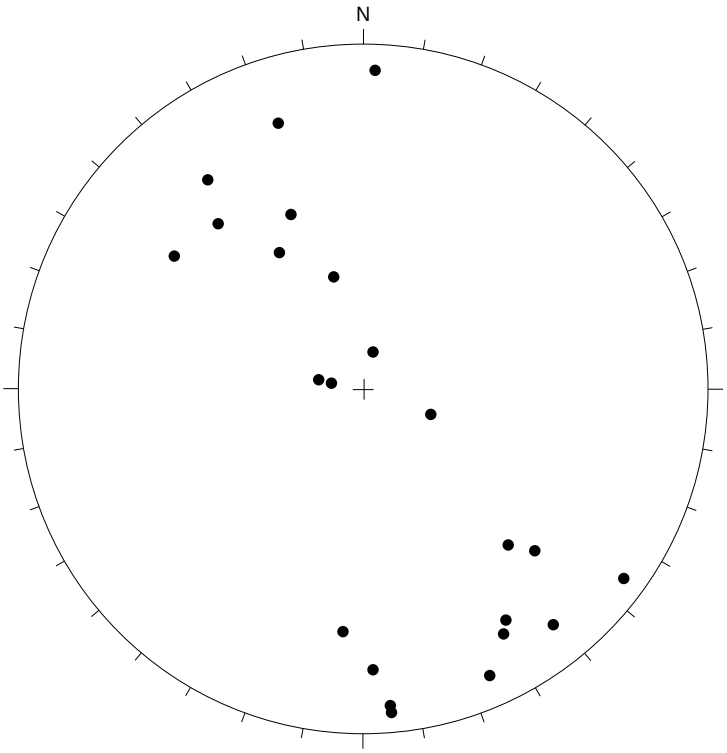

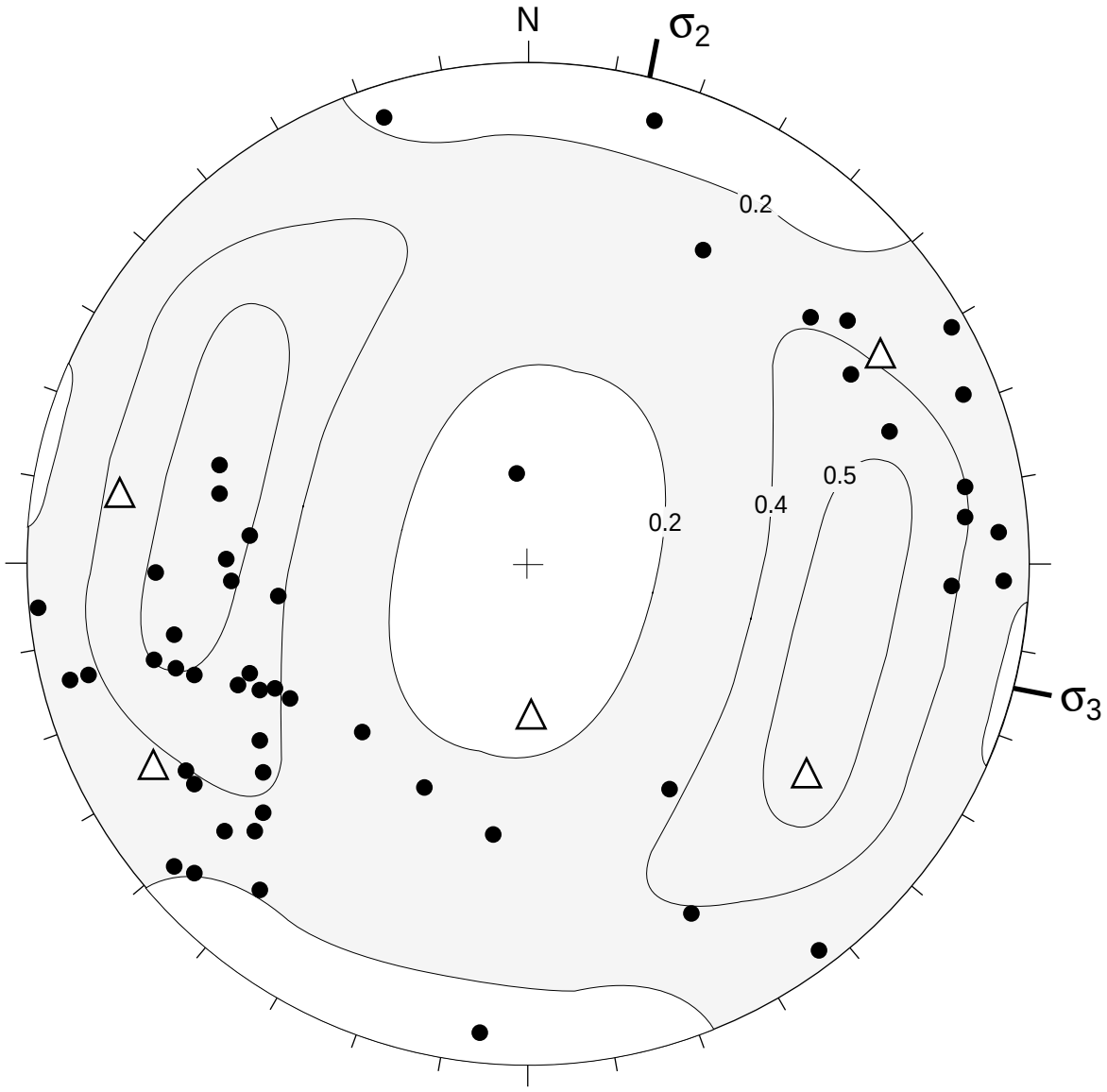
N
σ2
σ3
0.2
0.2
0.4
0.5

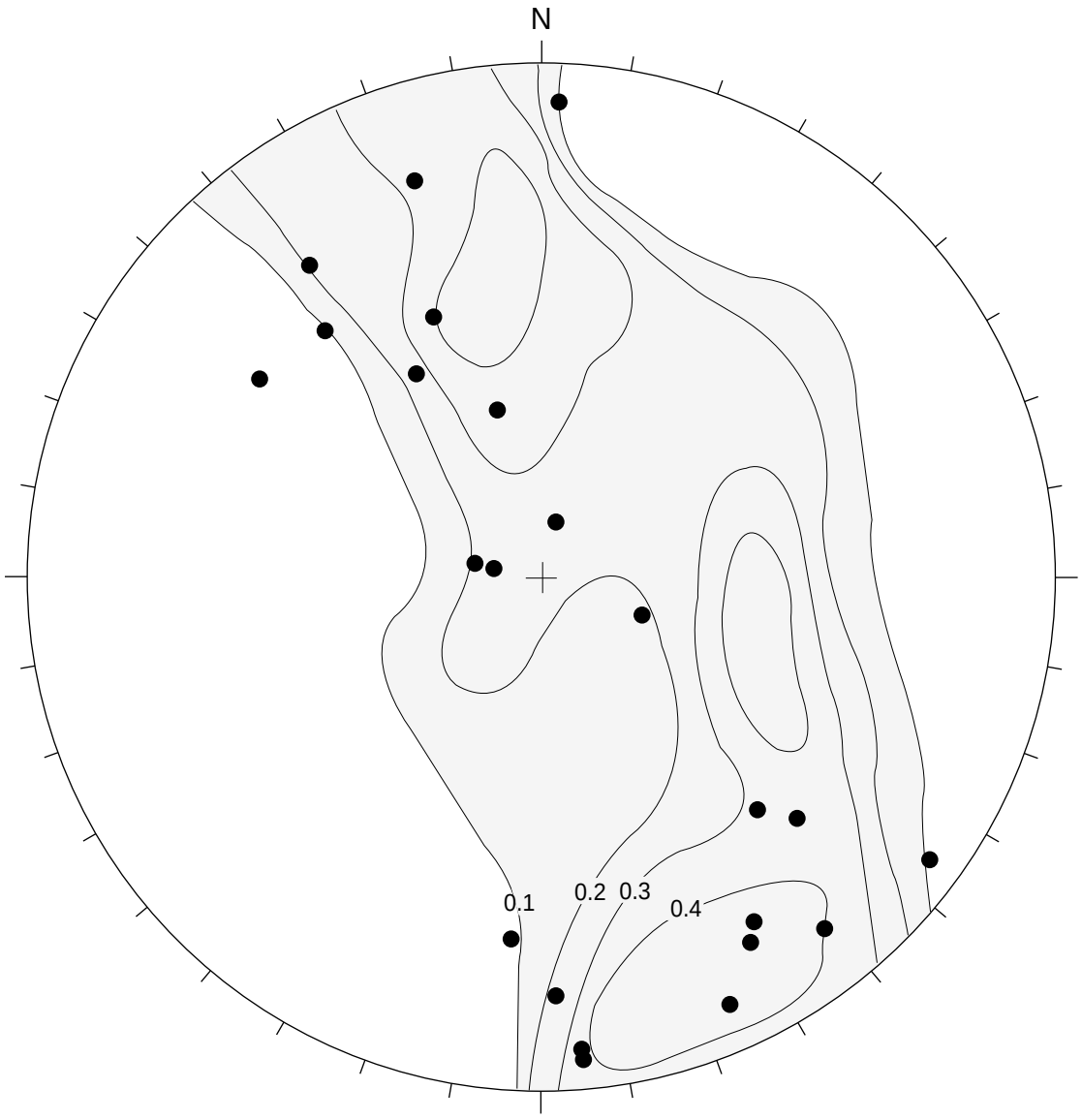
N
0.1
0.2
0.3
0.4